Hindawi
Adsorption Science & Technology
Volume 2021, Article ID 7896286, 14 pages
https://doi.org/10.1155/2021/7896286

Research Article

Electrochemical Determination of Diclofenac by Using ZIF-67/*g*-C_3N_4 Modified Electrode

Dang Thi Ngoc Hoa,[1,2] Nguyen Thi Thanh Tu,[3] Le Van Thanh Son,[4] Le Vu Truong Son,[4] Tran Thanh Tam Toan,[1] Pham Le Minh Thong,[5] Dao Ngoc Nhiem,[6] Pham Khac Lieu,[7] and Dinh Quang Khieu[1]

[1]*University of Sciences, Hue University, 53000, Vietnam*
[2]*University of Medicine and Pharmacy, Hue University, 55000, Vietnam*
[3]*Faculty of Technology, Van Lang University, 70000, Vietnam*
[4]*University of Education and Science, The University of Danang, 55000, Vietnam*
[5]*Institute of Research and Development, Duy Tan University, 55000, Vietnam*
[6]*Institute of Materials Science, Vietnam Academy of Science and Technology, 100000, Vietnam*
[7]*Hue University, 53000, Vietnam*

Correspondence should be addressed to Dinh Quang Khieu; dqkhieu@hueuni.edu.vn

Received 30 May 2021; Accepted 19 August 2021; Published 3 September 2021

Academic Editor: Thanh Son Le

A facial differential pulse voltammetric procedure using a glassy carbon electrode modified with zeolite imidazolate framework-67/graphitic carbon nitride (ZIF-67/*g*-C_3N_4) for the diclofenac (DCF) determination is demonstrated. ZIF-67/*g*-C_3N_4 with different mass ratios of the components was synthesized in a self-assembly process. The obtained materials were characterized by using X-ray diffraction, scanning electron microscopy (SEM), EDX-mapping, and nitrogen adsorption/desorption isotherms. The peak current varies linearly with the DCF concentration in the range of 0.2–2.2 μmol·L^{-1} and has a detection limit of 0.071 μmol·L^{-1}. The modified electrode exhibits acceptable repeatability, reproducibility, and selectivity towards DCF. The proposed electrode allows determining DCF in human urine without pretreatment, and the results are comparable with those determined with HPLC.

1. Introduction

Diclofenac, 2-(2′,6′-dicholoroanilino) phenylacetic acid (denoted as DCF), is used for the treatment of several diseases, such as ankylosing spondylitis, rheumatoid arthritis, and osteoarthritis [1]. However, diclofenac causes acute hepatotoxicity, and this chemical-driven liver damage leads to the change in the kidney function and gills in rainbow trout (O. mykiss). Diclofenac also presents acute toxicity to phytoplankton and zooplankton. Moreover, the possible synergetic effects with other pharmaceuticals or chemicals in the aquatic environment increase the environmental risk [2]. Various techniques have been developed to determine diclofenac because of the prominence of DCF in the environment and pharmaceutical and clinical applications. The techniques include capillary zone electrophoresis with electrochemical detection [3], high-performance liquid chromatography (HPLC) [4], HPLC combined with solid-phase extraction [5], and spectrofluorimetry [6]. Besides these techniques, electrochemical methods possess several advantages, such as high sensitivity, selectivity, and quick, cheap analysis for actual samples. These techniques use various types of porous materials to modify the working, such as ionic liquid/carbon nanotube-paste electrode [7], carboxyl/multiwalled carbon nanotubes/screen-printed carbon electrode [8], and gold/multiwalled carbon nanotube/glassy carbon electrode [9].

Zeolite imidazolate framework-67 (ZIF-67) is a subclass of metal-organic frameworks (MOFs). It is an organic-inorganic hybrid solid with infinite and uniform crystalline coordination networks consisting of cobalt ions (II) and imidazolate ligands [10]. ZIF-67 exhibits various unique properties, such as thermal and chemical stability, high surface area, large pores, accessible coordinative unsaturated sites, and excellent chemical and solvent stability [10]. At present, ZIF-67 attracts increasing attention from researchers in various fields, such as adsorption and separation [11], catalysis [12], and gas separation [13]. However, its poor electroconductivity leads to limited applications in electrochemistry [14]. Graphitic carbon nitride (g-C_3N_4) with graphitic-like structure possesses a unique ability to be simply prepared by thermally condensation of cheap nitrogen-rich compounds such as urea, melamine, and cyanimide [15, 16], and this is unlike graphene, reduced graphene oxide, and graphitic oxide that require the more complex synthesis processes. It has gradually attracted attention in multidisciplinary areas due to its characteristic physicochemical properties, such as ability to resist attacks from strong acid/alkaline solution [17], moderate bandgap (~2.7 eV), and superior electronic properties [18]. Therefore, the combination of highly electroconductive g-C_3N_4 with large surface area ZIF-67 might lead to versatile materials with properties of both components.

To the best of our knowledge, only a few papers have been reported on the voltammetric or amperometric detection of DCF on a ZIF-67/g-C_3N_4 modified electrode. Therefore, to fabricate new electrodes, we expand our research on modifying glassy carbon electrodes (GCE). In the present work, we describe the determination of DCF by using a GCE electrode modified with ZIF-67/g-C_3N_4. This modified electrode exhibits sound electrocatalytic and accumulative effects on DCF and enables us to determine the DCF content in human urine with satisfactory results.

2. Experimental

2.1. Materials. Melamine ($C_3N_3(NH_2)_3$), absolute ethanol (C_2H_5OH), methanol (CH_3OH), cobalt nitrate hexahydrate ($Co(NO_3)_2{\cdot}6H_2O$), and 2-methylimidazole ($CH_3C_3H_2N_2H$) were purchased from Merck company. Diclofenac sodium salt ($C_{14}H_{10}Cl_2NNaNO_2$) was procured from Sigma-Aldrich. Acetic acid (CH_3COOH), phosphoric acid (H_3PO_4), boric acid (H_3BO_3), and potassium hydroxide (KOH) were purchased from Daejung (Korea).

The phosphate buffer solution (PBS) with pH 7 was prepared from 0.5 M Na_2HPO_4, 0.5 M KH_2PO_4, 0.5 M NaCl, and 0.5 M KCl solutions. The Britton–Robinson buffer solution (B–RBS) with pH 3–9 was prepared from 1 M H_3BO_3, 1 M H_3PO_4, and 1 M CH_3COOH solutions and adjusted with a 1 M KOH solution. The stock solution was prepared by dissolving 29.6 mg of diclofenac in a 10 mL volumetric flask containing a pH 6 buffer solution. The flask was subjected to ultrasonication in a cold water bath and stored in a refrigerator at 5°C. The stock sample was prepared 30 min before analysis.

2.2. Material Synthesis. ZIF-67 was synthesized according to Qian et al. [10]. Briefly, 1.16 g of $Co(NO_3)_2{\cdot}6H_2O$ and 1.31 g of 2-methylimidazole (Hmim) were dissolved in 100 mL of methanol separately. These two solutions were mixed so that the resulting mixture has the following molar composition: Co^{2+}/Hmim/CH_3OH = 1 : 4 : 1.2 and stirred for 24 h at ambient temperature. Then, the purple solid (ZIF-67) was collected by centrifuging, washed with ethanol five times, and dried at 80°C for 24 h.

The g-C_3N_4 was synthesized according to Yan et al. [19]. In brief, 10 g of melamine powder was put into an alumina crucible with a cover and heated at 500°C in a muffle furnace for 2 h.

The ZIF-67/g-C_3N_4 was synthesized as follows: 0.5 g of the g-C_3N_4 and ZIF-67 mixture was distributed in 100 mL of ethanol under ultrasonication for 6 h. The ZIF-67/g-C_3N_4 mass ratio is as follows: 0 : 10, 3 : 7, 4 : 6, 5 : 5, 6 : 4, and 10 : 0. The samples are denoted as (0/10)ZIF-67/g-C_3N_4, (3/7)ZIF-67/g-C_3N_4, (4/6)ZIF-67/g-C_3N_4, (5/5)ZIF-67/g-C_3N_4, (6/4)ZIF-67/g-C_3N_4, and (10/0)ZIF-67/g-C_3N_4.

2.3. Instruments. The material was characterized by using X-ray diffraction (XRD) with a D8-Advance device (Bruker, USA; Cu Kα radiation, $\lambda = 1.5406$ Å), scanning electron microscopy (SEM) with JMS-5300LV (USA), Raman spectroscopy with Xplora Plus (Horiba with 785 nm laser excitation), transmission electron microscopy (TEM) with JEM-2100, and nitrogen adsorption/desorption isotherms with a Micromeritics 2020 volumetric adsorption analyzer system (the sample was degassed at 150°C for 12 h). The specific surface area was calculated according to the Brunauer–Emmett–Teller (BET) model. The meso/micro-surface area was calculated with the t-plot method. Electrochemical measurements were conducted with a CPA-HH5 computerized polarography analyzer (Vietnam). A three-electrode system consisting of a working electrode (GCE, 0.28 cm^2), a reference electrode (Ag/AgCl in saturated KCl), and a counter electrode (platinum wire) was used for the measurements. The high-performance liquid chromatography (HPLC) was performed to measure DLF for the sake of comparison. The HPLC measurements were conducted on an HPLC Shimadzu with LC 20 AD pump, PDA SPD–M20A detector (Japan), C18 column (250 × 4.6 mm; particle size 5 μm). The mobile phase is a mixture of methanol/5 mM NaH_2PO_4 (pH 2.3) (66 : 34 v/v). The flow rate was 1 mL·min^{-1} with an injection volume of 20 μL. For HPLC analysis, DCF detection was performed at a wavelength of 274 nm.

2.4. Preparation of Electrode and Actual Sample

2.4.1. Electrode Preparation. Prior to modification, the GCE was first polished with alumina slurry (0.05 μm) on a polishing pad, followed by successive ultrasonication in ethanol and distilled water. Then, the electrode was washed with double distilled water and dried at ambient temperature. The suspension of ZIF-67/g-C_3N_4 was prepared by mixing 10 mg of ZIF-67/g-C_3N_4 with 10 mL of ethanol under ultrasonication for 24 h. Five microliters of suspension was cast dropwise on the GCE surface and dried in an oven for a

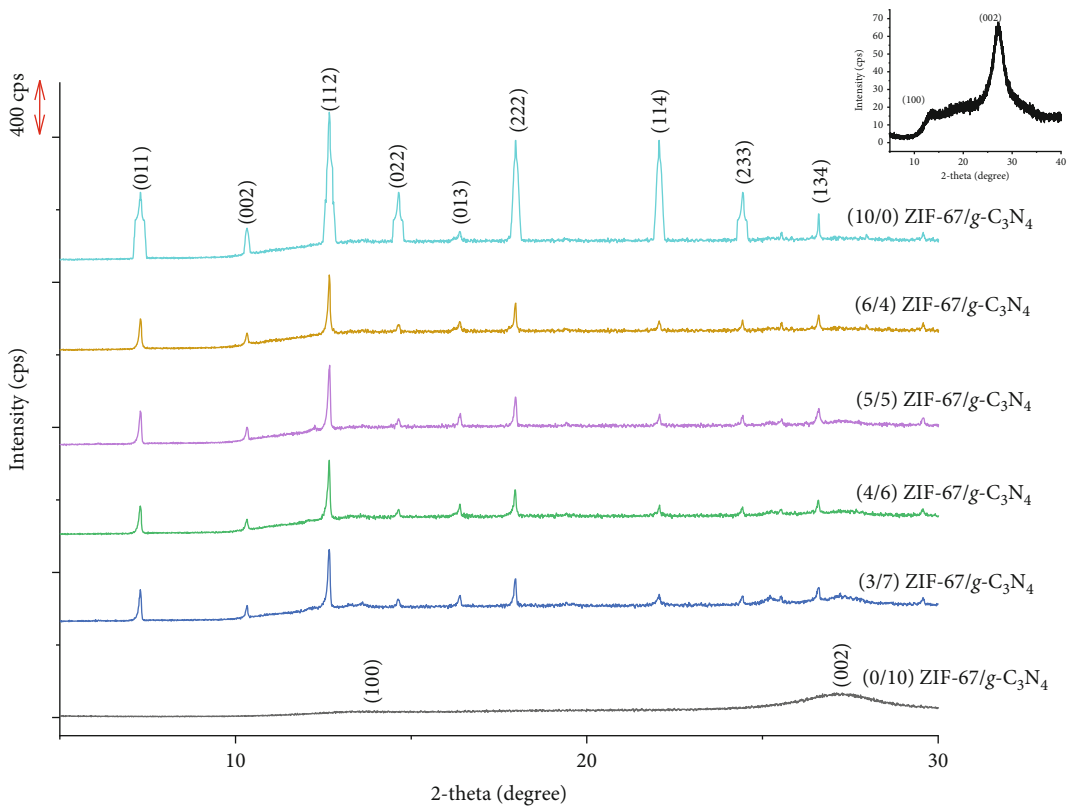

Figure 1: XRD patterns of ZIF-67, g-C_3N_4, and ZIF-67/g-C_3N (the inset presents the XRD partten of (0/10)ZIF-67/g-C_3N_4).

few minutes. The *as*-prepared electrode was denoted as ZIF-67/g-C_3N_4-GCE.

2.4.2. Real Samples. Human urine samples were received from five healthy persons aged 25–30 and stored in a refrigerator at 5°C. About 5 mL of the sample was filtered through a 0.2 μm membrane. One milliliter of the supernatant was collected and diluted with 2 mL of pH 6.5 BRS to avoid complex interference. The resulting solution was transferred to a 100 mL electrochemical cell for analysis.

3. Results and Discussion

3.1. Characterization of Materials. The XRD patterns of g-C_3N_4, ZIF-67, and ZIF-67/g-C_3N_4 are shown in Figure 1. Two peaks at around 13.7 and 27.1° are found in g-C_3N_4 ((0/10)ZIF-67/g-C_3N_4)). It is well known that g-C_3N_4 consists of tri-s-triazine building blocks [20]. The higher peak at 27.1° is assigned to the characteristic interlayer of aromatic systems, indexed for graphitic materials as (002), while the peak at 13.7°, indexed as (100), is attributed to the periodic arrangement of the condensed tri-s-triazine units in the sheets [21] (the inset of Figure 1). For the XRD pattern of (10/0)ZIF-67/g-C_3N_4, the characteristic peaks for ZIF-67 at 18.20, 30.22, 35.68, 43.28, 53.68, 57.18, and 62.76°, indexed as (111), (220), (311), (400), (422), (511), and (440) according to CCDC 671073, are clearly observed indicating that the (10/0)ZIF-67/g-C_3N_4 is ZIF-67. The intensity of these peaks in ZIF-67/g-C_3N_4 increases with an increase in the ZIF-67/g-C_3N_4 fraction. This increase manifests the coexistence of g-C_3N_4 and ZIF-67 phases in the composite. Clear characteristic peaks of ZIF-67 witness that the hybrid of ZIF-67 with g-C_3N_4 has no significant effects on the crystal structure of ZIF-67.

Nitrogen adsorption/desorption isotherms are employed to evaluate the samples' specific surface area and porosity (Figure 2). The isotherm curves of ZIF-67 have a type I isotherm, indicating the presence of a microporous material. The g-C_3N_4 has a type IV isotherm with an H3 hysteresis loop at high relative pressure between 0.46 and 1.0, confirming the existence of a mesoporous structure. The BET surface area (S_{BET}) and total pore volume (V_{pore}) are listed in Table 1.

Compared with pure ZIF-67, the ZIF-67/g-C_3N_4 has the S_{BET} declining from 1217.1 to 335.6 $m^2 \cdot g^{-1}$ as the amount of g-C_3N_4 increases. This decline might result from the low surface area of g-C_3N_4 and blockage of micropores of the increasing g-C_3N_4 amount in the composite. The primary test reveals that the (5/5)ZIF-67/g-C_3N_4 sample has the highest electrocatalytic activity for DCF oxidation. Therefore, (5/5)ZIF-67/g-C_3N_4 is selected for further experiments.

As shown in Figure 3(a), smooth rhombic dodecahedral-shaped crystals with 1.5 μm in width are observed for ZIF-67. The surface of g-C_3N_4 exhibits a layered and platelet-like morphology (Figure 3(b)). Although several inclusions of g-C_3N_4 appear on the ZIF-67 surface, the rhombic dodecahedral structure of ZIF-67 remains (Figure 3(c)). The TEM image illustrates a sheet-like structure of g-C_3N_4 embroiled with dark-colored ZIF-67 crystals

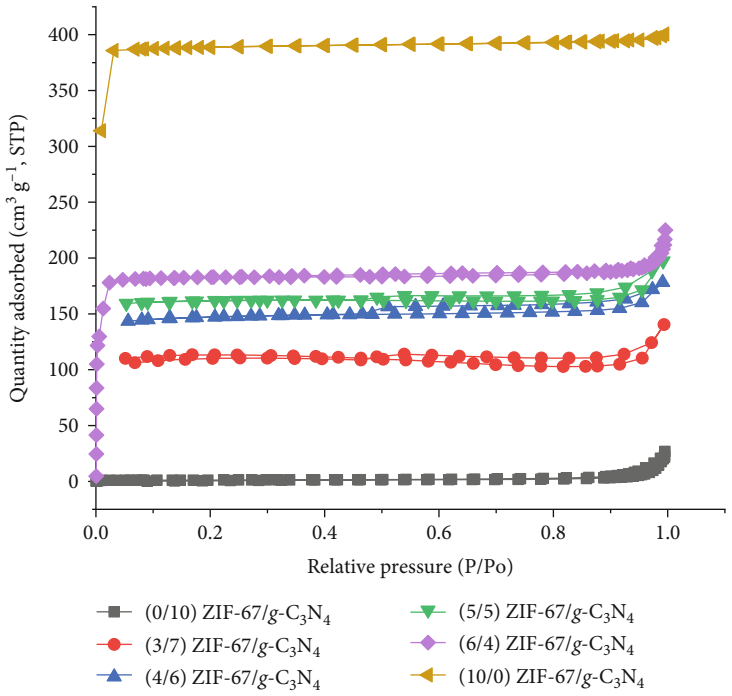

Figure 2: Nitrogen adsorption/desorption isotherms of ZIF-67, g-C_3N_4, and ZIF-67/g-C_3N_4.

Table 1: Textural properties of ZIF-67/g-C_3N_4.

Notation	S_{BET} ($m^2 \cdot g^{-1}$)	S_{meso} ($m^2 \cdot g^{-1}$)	S_{micro} ($m^2 \cdot g^{-1}$)	V_{total} ($cm^3 \cdot g^{-1}$)
(0/10)ZIF-67/g-C_3N_4	4.2	2.7	1.5	26.9
(3/7)ZIF-67/g-C_3N_4	335.6	25.1	310.5	140.4
(4/6)ZIF-67/g-C_3N_4	449.0	9.8	439.2	197.3
(5/5)ZIF-67/g-C_3N_4	492.0	10.5	481.5	178.2
(6/4)ZIF-67/g-C_3N_4	731.9	10.6	721.3	225.0
(10/0)ZIF-67/g-C_3N_4	1217.1	6.9	1210.1	400.6

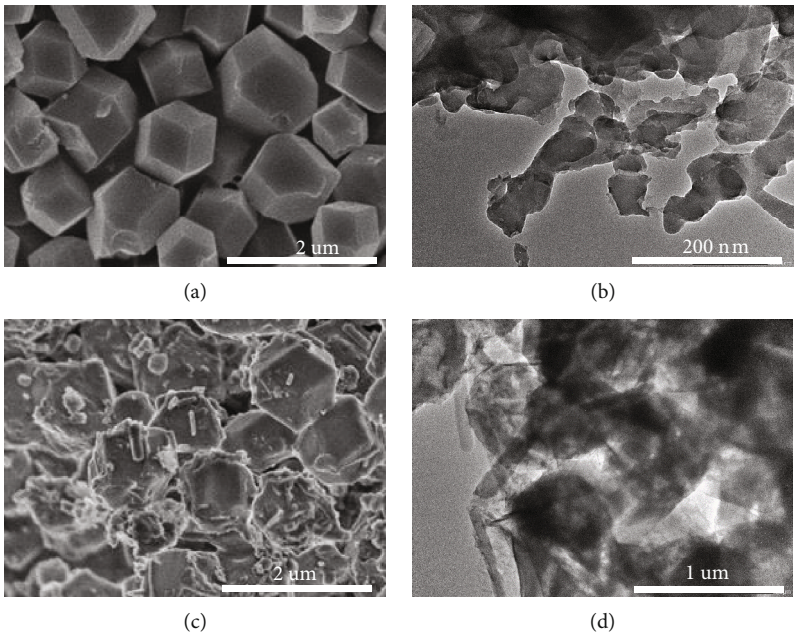

Figure 3: (a) SEM image of ZIF-67, (b) TEM image of g-C_3N_4, (c) SEM image of ZIF-67/g-C_3N_4, and (d) TEM image of (5/5)ZIF-67/g-C_3N_4.

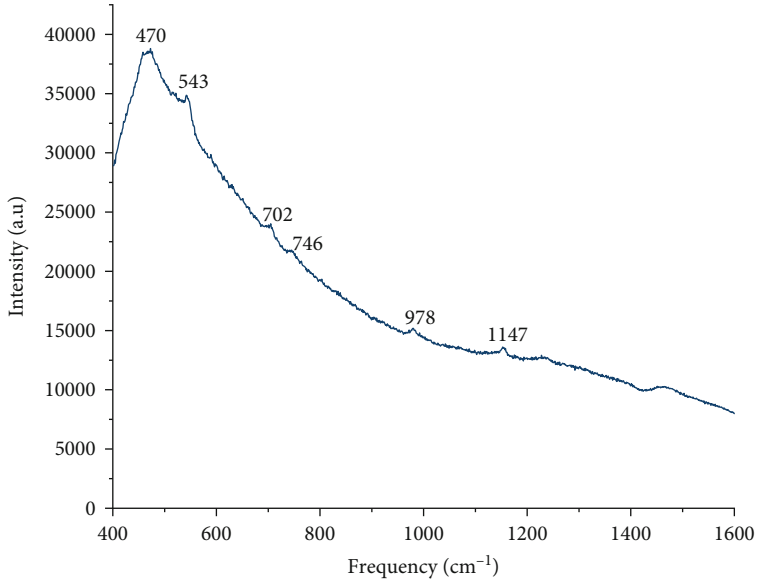

(a)

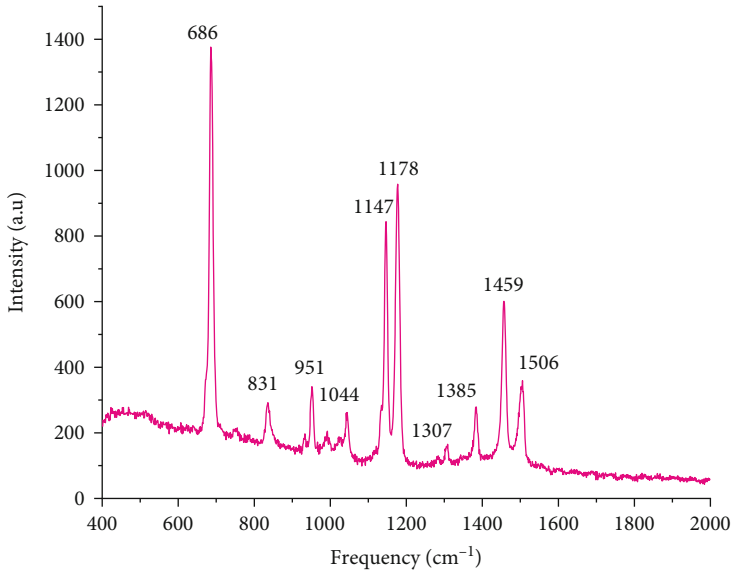

(b)

Figure 4: Continued.

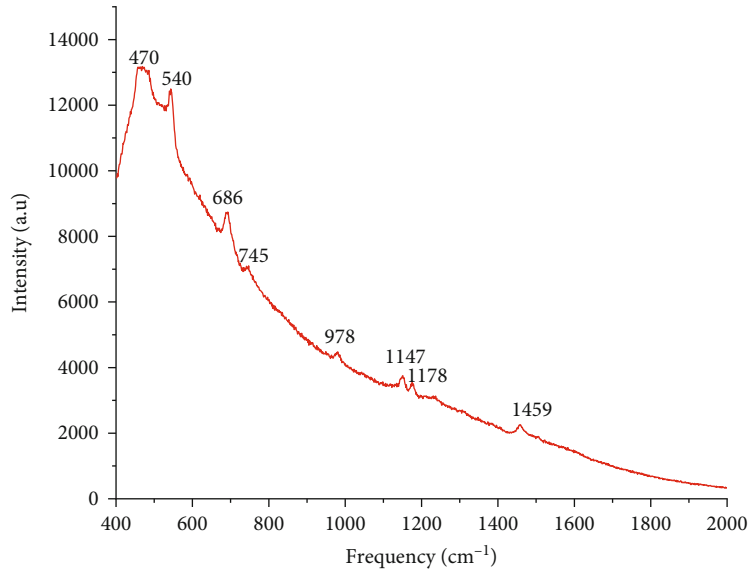

Figure 4: Raman spectra of (a) g-C_3N_4, (b) ZIF-67, and (c) ZIF-67/g-C_3N_4.

(Figure 3(d)). These results indicate the coexistence of ZIF-67 and g-C_3N_4 via self-assembly.

The ZIF-67/g-C_3N_4 structure is characterized by using Raman spectra (Figure 4). Typical characteristic peaks of g-C_3N_4 at 470, 543, 702, 746, 978, and 1147 cm^{-1} are observed, and they are consistent with those in a previously published report [22]. The peaks at 702 and 978 cm^{-1} indicate the existence of the heptazine ring structure [23]. The peak at 702 cm^{-1} is ascribed to the inplane bending vibrations of the heptazine linkages, whereas the 978 cm^{-1} peak is assigned to the symmetric N-breathing mode of the heptazine units [24]. For ZIF-67, characteristic peaks at 686, 831, 951, 1044, 1147, 1178, 1307, 1385, 1459, and 1506 cm^{-1} are attributed to the cobalt ion [25], imidazolium ring puckering, δ H (out of plane), bending C–H (out of plane) (C4–C5), bending C–H (out of plane) (C2–H), stretching C–N, N–H wag, bending of CH_3, stretching of C2–N1, and stretching of C–H (methyl), respectively [26]. The characteristic vibrations of ZIF-67 and g-C_3N_4 in the Raman spectrum of ZIF-67/g-C_3N_4 confirm the coexistence of ZIF-67 and g-C_3N_4 again.

The elemental composition of ZIF-67/g-C_3N_4, derived from the EDX spectrum, is presented in Figure 5. As expected, the elements in (5/5)ZIF-67/g-C_3N_4 are only carbon (at 0.3 keV), nitrogen (0.4 keV), oxygen (0.6 keV), and cobalt (0.8; 7.0; 7.7 keV), indicating that the obtained material has high purity (Figures 5(a) and 5(b)). The EDX mapping of carbon (Figure 5(c)), cobalt (Figure 5(d)), nitrogen (Figure 5(e)), and oxygen (Figure 5(f)) on the ZIF-67/g-C_3N_4 surface shows that all these elements are not confined to a single site. Instead, they are distributed in the matrix.

Although Figure 6 shows that ZIF-67 could attach to the surface of g-C_3N_4, such self-assembly can be further confirmed by studying the surface charges of ZIF-67, g-C_3N_4, and their composite (Figure 6). These values are determined with the drift pH method [27]. As seen from the figure, the material's surface is positively charged when pH < 9.2 for ZIF-67 and pH < 3.8 for g-C_3N_4. Therefore, the electrostatic attraction between ZIF-67 and g-C_3N_4 could form ZIF-67/g-C_3N_4 with a positively charged surface at pH below 8.4.

The stability of (5/5)ZIF-67/g-C_3N_4 in the solutions with different pHs is essential for the electrochemical application. Figure 7 presents the XRD patterns of (5/5)ZIF-67/g-C_3N_4 immersed in water with different pHs for 5 hours. At pH less than 4, the characteristic diffractions of ZIF-67 are absent, revealing that the material is destroyed at these pHs. The peaks of ZIF-67 remain in the solutions with pH 5–10, indicating that ZIF-67 is stable in this pH range.

3.2. Electrochemical Determination of Diclofenac by Using (5/5)ZIF-67/g-C_3N_4

3.2.1. The Cyclic Voltammetry of DCF on (5/5)ZIF-67/g-C_3N_4 Modified Electrode (ZC-GCE). The cyclic voltammograms (CVs) (Figure 8) are obtained in the presence of 5 mM DCF on GCE, ZIF-67-GCE, g-C_3N_4-GCE, and ZIF-67/g-C_3N_4-GCE in 0.2 M BRS pH 6. The bare GCE does not exhibit any electrochemical signals, indicating that this electrode cannot detect DCF. The modified electrodes (with ZIF-67, g-C_3N_4, or ZIF-67/g-C_3N_4) exhibit an oxidation peak of DCF at around 0.68 V. In particular, the ZIF-67/g-C_3N_4 modified electrode significantly enhances the electrochemical response, and the intensity of peak current depends on the ZIF-67 and g-C_3N_4 mass ratio. The (5/5)ZIF-67/g-C_3N_4-GCE (henceforth denoted as ZC-GCE) provides the highest intensity with a peak potential of 0.671 V. The peak current is 2.1-fold and 2.12-fold higher than that of g-C_3N_4/GCE and ZIF-67-GCE, respectively. The substantial enhancement in the anodic peak current clearly shows the catalytic effect of ZIF-67/g-C_3N_4. No reduction peaks are observed on the reverse scan, indicating that the electron transfer on the ZC modified electrode is

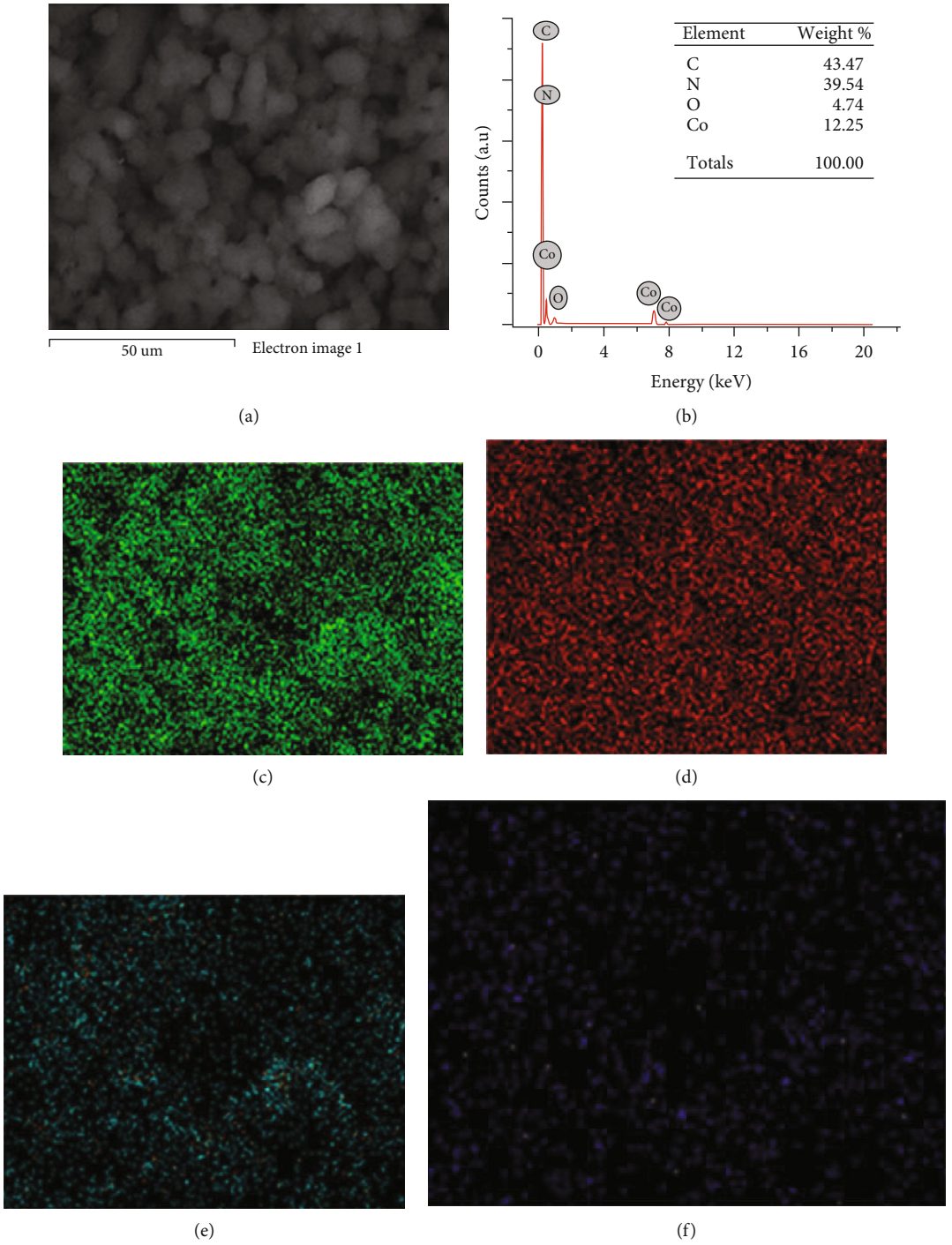

FIGURE 5: EDX-mapping of electron image for ZIF-67/g-C_3N_4 (a, b), carbon element (c), cobalt element (d), nitrogen element (e), and oxygen element (f).

irreversible. In addition, the ZC-GCE does not exhibit an oxidation/reduction peak on the voltammogram in the solution without DCF, indicating the ZC-GCE is inactive in the studied potential range.

(1) Effect of pH. The influence of pH on the oxidation peak current of the 5.0×10^{-3} M DCF solution is studied by using CV in the BR buffer. At pH 3–5, DCF oxidation at the electrode is not observed. It is possibly due to the unstable structure of ZIF-67 in ZIF-67/g-C_3N_4 in this pH range (Figure 7). The peak current increases with pH and has the highest value at pH 6.5. Higher pHs witness a decrease of the peak current up to pH 8, and then the current increases again (Figure 9(c)). Therefore, pH 6.5 is selected for further experiments. The point of zero charge of ZIF-67/g-C_3N_4 is 8.4, and the pK_a of DCF is around 4 [28]. The pH dependence

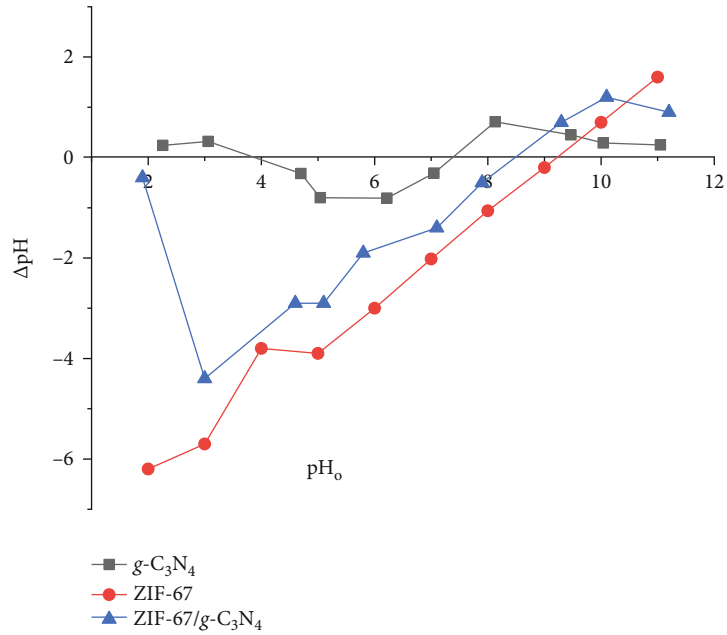

Figure 6: Point of zero charge (pH_{PZC}) of (5/5)ZIF-67/g-C_3N_4, ZIF-67, and g-C_3N_4.

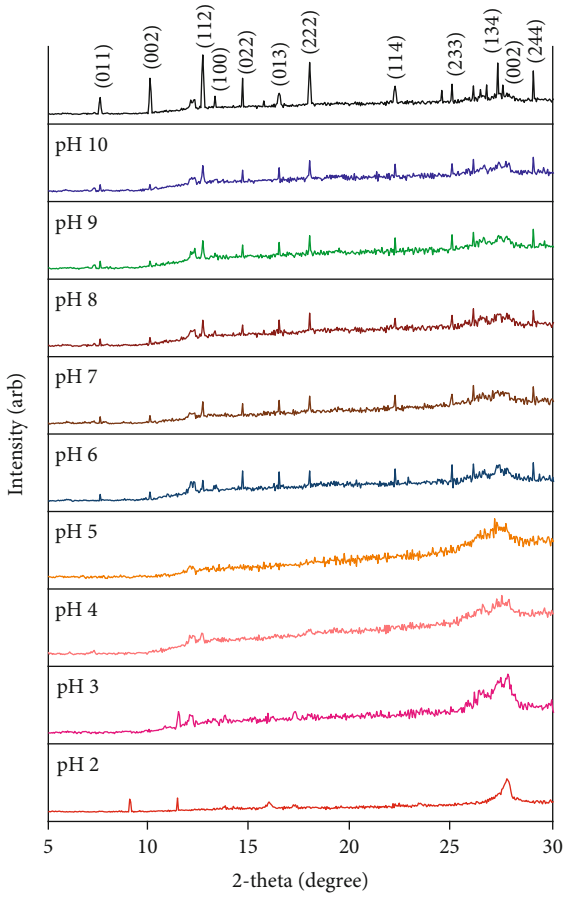

Figure 7: XRD patterns of (5/5)ZIF-67/g-C_3N_4 at pH 2–10.

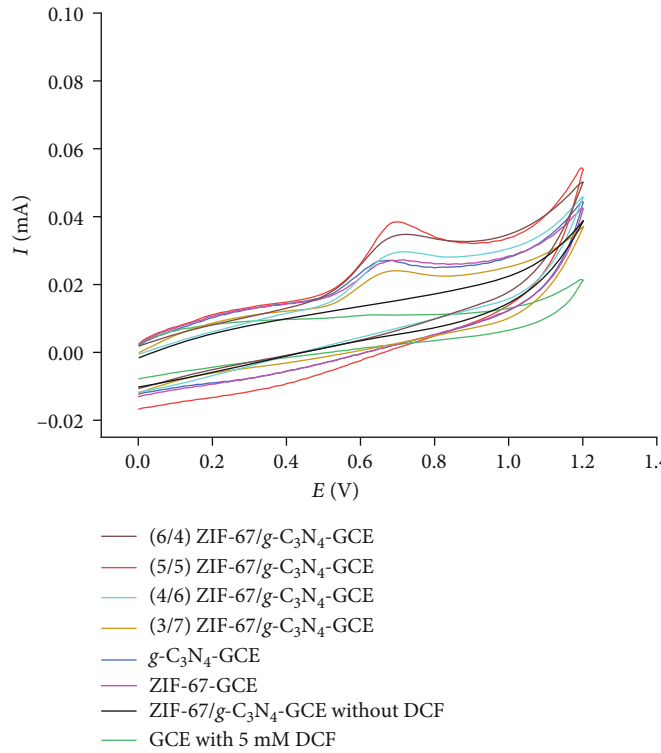

Figure 8: Cyclic voltammograms of 5 mM DCF in 0.2 M BRB pH 6 on GCE, ZIF-67-GCE, g-C_3N_4-GCE, and ZIF-67/g-C_3N_4-GCE.

of peak currents of DCF oxidation could not be explained by the electrostatic interaction between charged species on the opposite sites. This process may follow a mechanism different from electrostatic interaction.

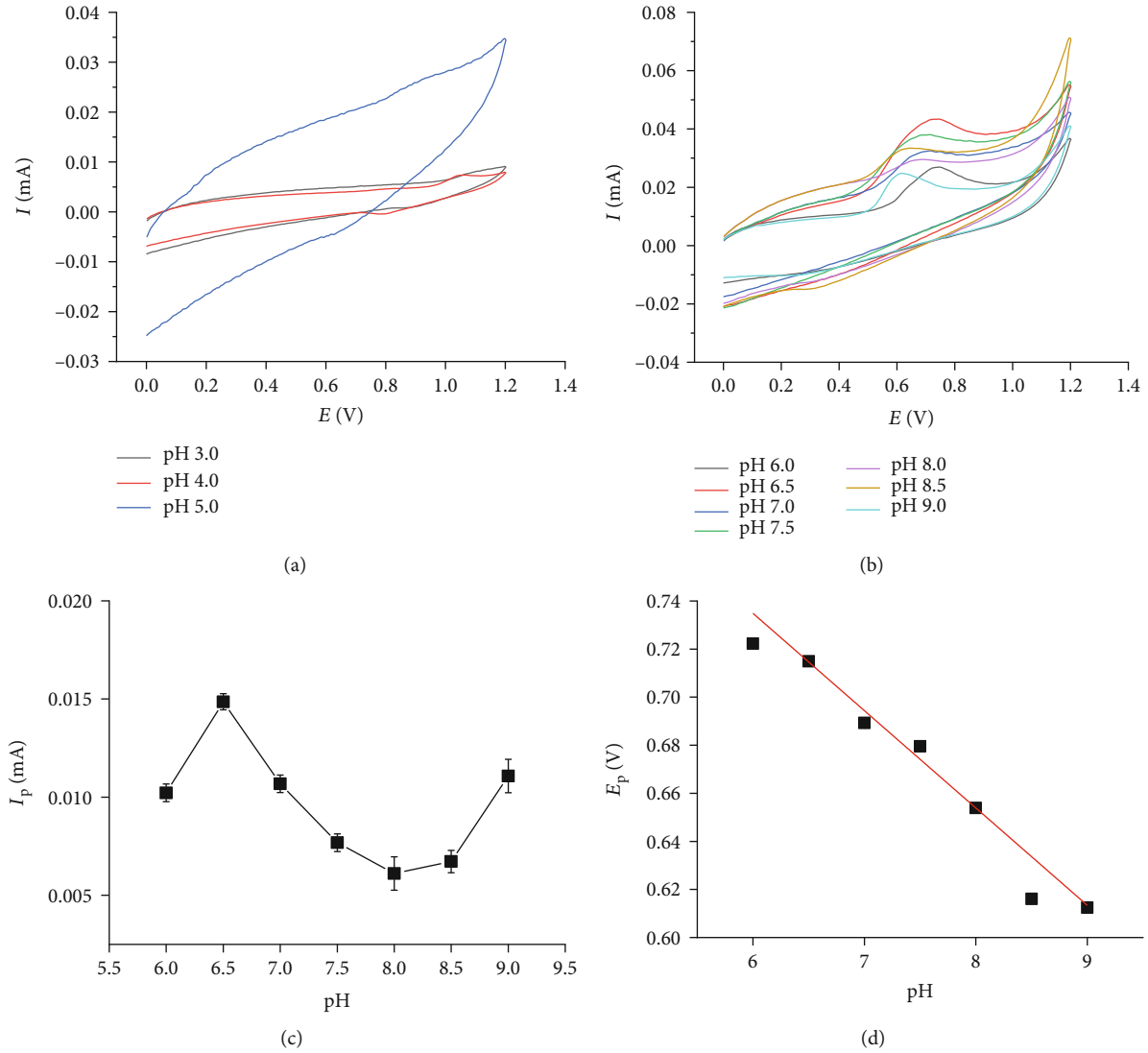

Figure 9: CVs of 5 mM DCF with (a) pH 3–5, (b) pH 6–9 in 0.2 M BRB, (c) I_p vs. pH, and (d) E_p vs. pH.

When pH is greater than 5, the peak potential decreases, suggesting the involvement of protons in the oxidation reaction (Figure 9(d)). The peak potential in the DCF oxidation on the ZC-GCE decreases linearly with the pH of the buffer solution according to the following equation: $E_{pa}\,(\mathrm{V}) = -0.0514 \times \mathrm{pH} + 0.9409\ (r^2 = 0.9988)$. The slope of the equation is close to the Nernstian value (−0.0592 mV) for the electrochemical processes involving an equal number of protons and electrons.

(2) Effect of Scan Rate. The scan rate of CVs is chosen from 0.1 to 0.5 $\mathrm{mV{\cdot}s^{-1}}$. In this range, the anodic peak current increases (Figure 10(a)). The highly linear relationship between I_p and the scan rate manifests that the electrode process is predominantly controlled by adsorption [29] (Figure 10(b)). The scan rate effect is also examined from the function $I_p = f(v^{1/2})$ plot. A straight line passing the origin suggests an adsorption-controlled electrode process [30]. This relationship in our study is $I_p = (0.003 \pm 0.011) + (0.028 \pm 0.006) \times v^{1/2}$; $r = 0.927$. With the 95% confident interval, the intercept passes 0 (between −0.008 and 0.014) and confirms an adsorption-controlled process again.

The relationship between the peak potential and the natural logarithm of the scan rate can provide the number of electrons transferred (n) on the electrode surface. For an irreversible system, this relationship is described by Laviron's equation [31]:

$$E_p = E^0 - \frac{R \times T}{(1-\alpha) \times n \times F} \times \ln \frac{R \times T \times K_s}{(1-\alpha) \times n \times F} + \frac{R \times T}{(1-\alpha) \times n \times F} \times \ln v, \quad (1)$$

where α is the electron-transfer coefficient, K_s is the apparent charge-transfer rate constant, n is the number of electrons transferred, v is the scan rate ($\mathrm{V{\cdot}s^{-1}}$), $R = 8.314\ \mathrm{J \cdot mol^{-1} \cdot K^{-1}}$, and $F = 96500\ \mathrm{C \cdot mol^{-1}}$ at 298 K. The linear regression of E_p versus $\ln(v)$ is as follows:

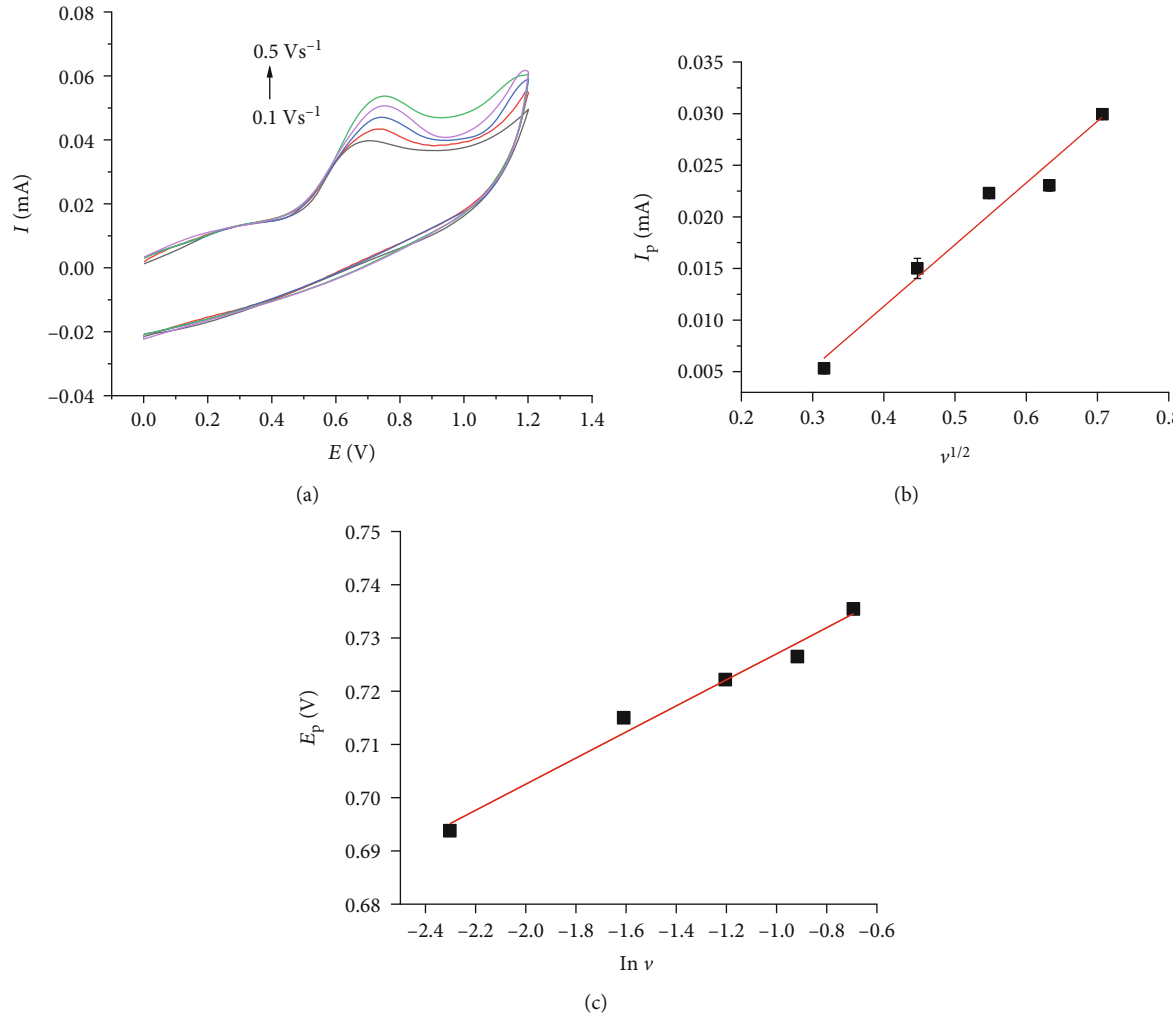

Figure 10: CVs of 5 mM DCF at various scan rates in 0.2 M BRS pH 6.5 on ZIF-67/g-C_3N_4 (a), the plot of I_p vs. $v^{1/2}$ (b), and E_p vs. ln$v$ (c).

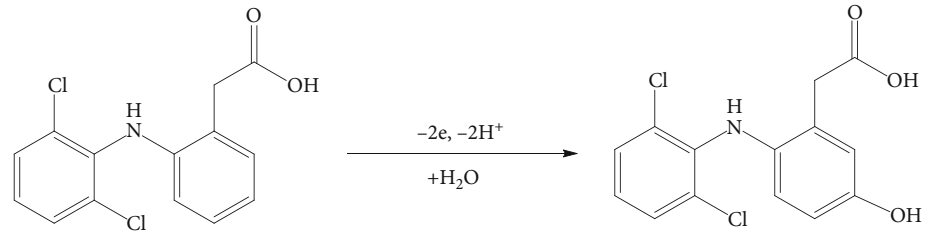

Scheme 1: Oxidation mechanism of DCF on ZC-GCE.

$$E_p = (0.751 \pm 0.002) + (0.025 \pm 0.001) \times \ln\ v\,;\, r = 0.991. \quad (2)$$

The value of $(1-\alpha) \times n$ calculated from the slope of this straight line is 0.95. For an irreversible system, α is considered as 0.5 [32]; therefore, the value of n is equal to 1.9 (≈2). Considering the pH effect on the anodic peak current, we can conclude that the redox reaction on the modified electrode involves the transfer of two electrons and two protons.

These results are consistent with those reported by Madsen et al. [33] and Goyal et al. [34], in which DCF is oxidized to 5-hydrodiclofenac via losing two electrons and two protons, as shown in Scheme 1.

The enhancement of electrochemical signals could result from the synergic effect of ZIF-67 and g-C_3N_4. The open Co(II) sites, as a Lewis acid [35], could attract the carboxyl group in DCF, and as a Lewis base via acid-base interaction, the graphitic rings in g-C_3N_4 could attract the benzene rings in DCF via π–π interaction. These arguments are schematically illustrated in Scheme 2.

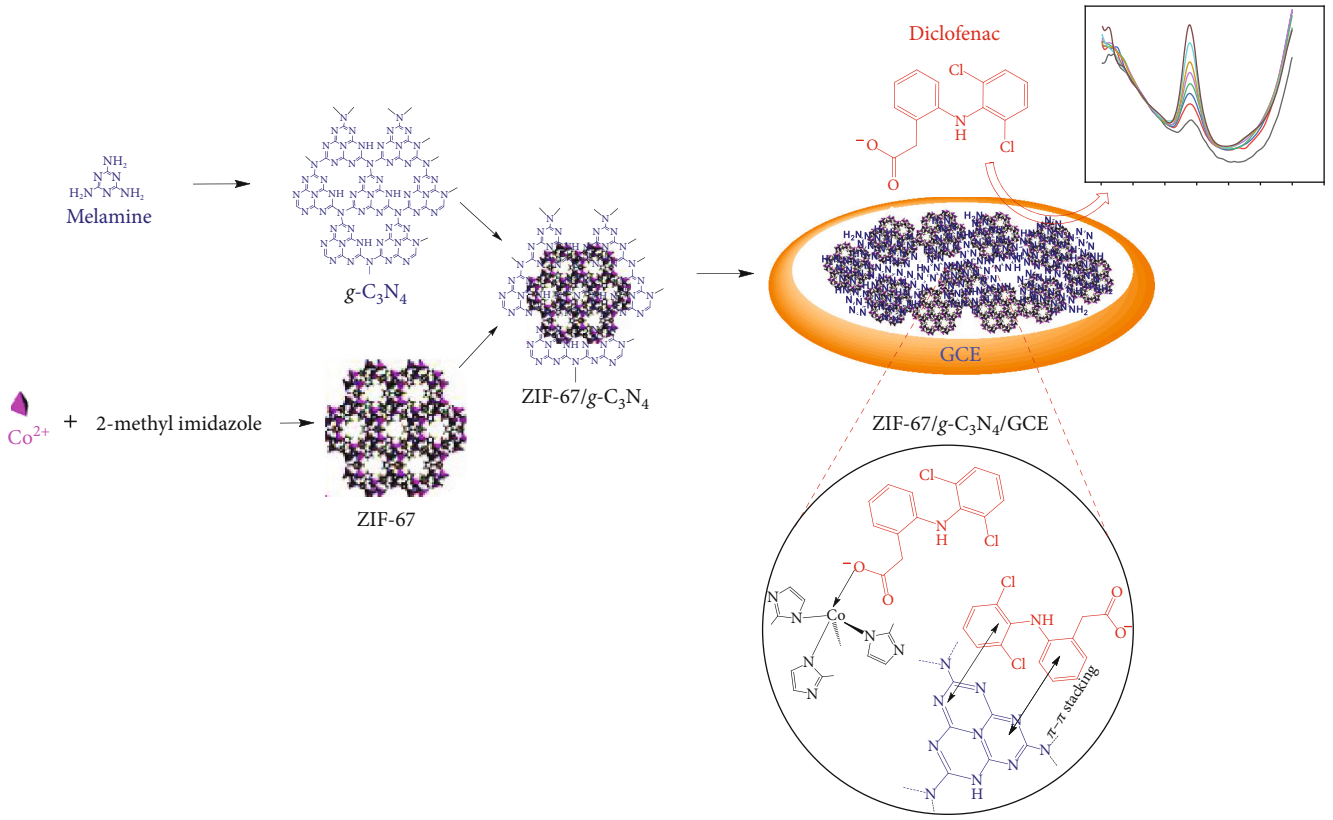

Scheme 2: Schematic illustration of the formation of ZIF-67/g-C_3N_4 modified GCE and its oxidation of DCF.

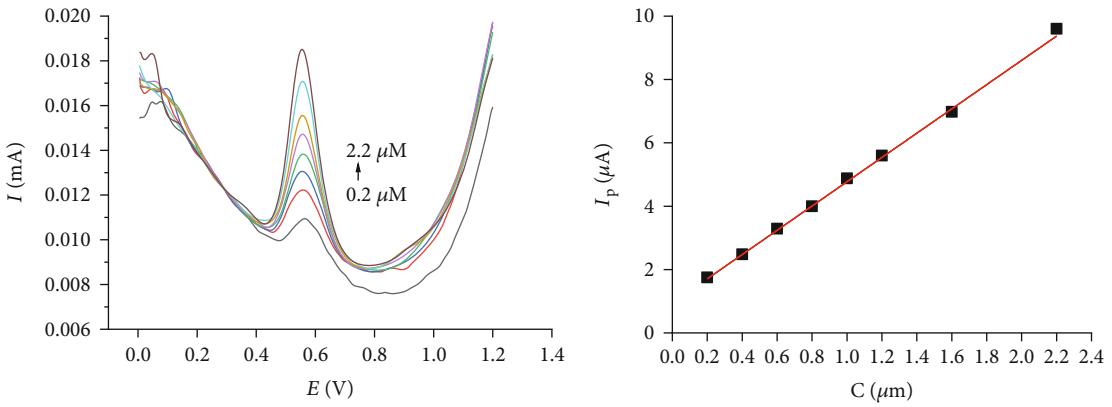

Figure 11: DPV curves of DCF with different concentrations (0.2–2.2 μM) in 0.2 M BRS pH 6.5 at the modified electrode (a). The plot of I_p vs. concentration (b).

3.2.2. Linear Range, Detection Limit, Repeatability, and Interference

(1) Linear Range and Detection Limit. The relationship between the peak current and DCF concentration is studied by using differential pulse voltammetry (DPV). In this case, the peak current increases linearly with the concentration of DCF, from 0.2 to 2.2 μM (Figure 11). The regression equation is $I_p = (0.941 \pm 0.02) + (3.889 \pm 0.03) \times C$; $r = 0.999$. The LOD ($3S/n$) is 0.071 μM. The detection limit, the linear range, and the sensitivity of the proposed DPV method are compared with previously reported values for the determination of DCF (Table 2). Although the proposed electrode has a relatively narrow linear range, it has high sensitivity and a lower detection limit. This method can be used to determine DCF in pharmaceuticals and water samples in the micromole range.

(2) Reproducibility and Repeatability. The reproducibility is studied from four replicates measurements of DCF determination. To investigate the repeatability of this modified electrode, we conduct the measurements ten times with the

Table 2: Comparison of the analytical performance of the different modified electrodes for the determination of DCF.

Electrodes	Technique	Linear range (μM)	LOD (μM)	References
Gold nanoparticle/multiwalled carbon nanotube modified glassy carbon electrode	SWV	0.03–200	0.02	[9]
Cu-doped zeolite-expanded graphite-epoxy electrode	DPV	0.3–20	0.05	[36]
APTES-amino-AT-silica/GCE	SWV	0.3–20	0.053	[37]
Gold nanoparticles decorated multiwalled carbon nanotubes/graphene oxide/AuE	DPV	0.4–80	0.09	[38]
Ionic liquid modified carbon nanotube paste electrode	DPV	0.5–300	0.2	[7]
Amino-AT/GCE	SWV	0.3–20	0.204	[37]
Au-Pt bimetallic nanoparticles decorated multiwalled carbon nanotubes/gold electrode	DPV	0.5–1000	0.3	[39]
ZIF-67/g-C_3N_4	DPV	0.2–2.2	0.071	The present work

Square wave voltammetry: SWV.

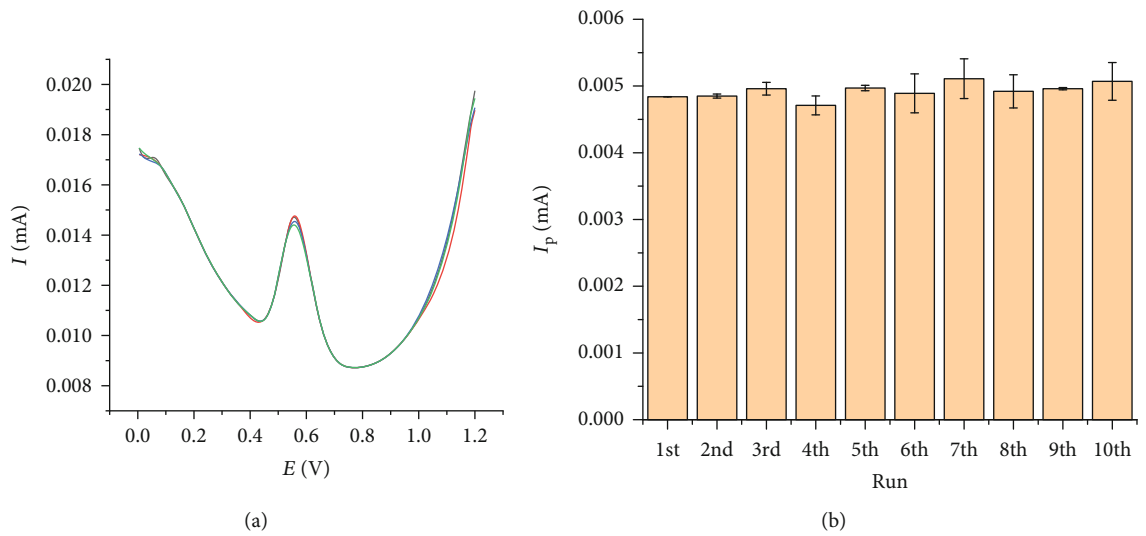

Figure 12: The DPV of four replicates measurement (a) and the values of peak current of DCF on ZC-GCE modified using (5 μL ZC (1 mg/mL) for ten times on the same electrode (b).

sample electrode. Figure 12(a) shows very similar DPV curves of four scans on the same working electrode. The small RSD of 1.32% indicates good reproducibility of the proposed method. Figure 12(b) presents the values of peak currents measured on 10 distinct working electrodes under the same modified electrode procedure. The RSD varies from 0.151% to 5.315% in run 1 to run 10, manifesting excellent repeatability.

The biological sample is a very complex mixture consisting of various ions and molecules. Possible interfering electroactive species on the biological samples include inorganic salts ($KHCO_3$, Na_2SO_4, $CaCl_2$, and NH_4NO_3) and organic compounds (uric acid, caffeine, paracetamol, and ascorbic acid). Table 3 reveals that inorganic salts do not significantly interfere with the measurement even at extremely high content (100–320 fold). Ascorbic acid does not seem to affect the peak current at 480-fold concentration. Paracetamol, uric acid, and caffeine exert a medium effect on the peak current at a concentration of 40 to 80-fold higher than that of DCF. These results confirm the relevant selectivity of the proposed method for DCF detection.

Table 3: Effect of some foreign substances on the determination of 1 μM DFC in 0.2 M BRBS pH 6.5.

Interferents	Tolerance level (M/M)	Rev. (%)
$KHCO_3$	320	6.80
Na_2SO_4	480	13.57
$CaCl_2$	320	12.86
NH_4NO_3	80	6.58
Uric acid	80	6.34
Caffeine	80	10.14
Paracetamol	40	5.13
Ascorbic acid	480	9.38

Table 4: The results of DCF analysis in urine by the proposed DPV method and HPLC.

Sample	DPV analysis			Rev (%)	HPLC analysis	
	Original content (μM)	Spiked (μM)	Found (μM)		Original content (μM)	Found (μM)
Urine 1	—	50	51.243 ± 0.229	102.49	—	48.931 ± 0.015
Urine 2	—	50	48.102 ± 0.085	96.20	—	47.823 ± 0.204
Urine 3	—	50	49.215 ± 0.081	98.43	—	50.387 ± 0.139
Urine 4	0.257 ± 0.074	50	54.013 ± 0.167	104.96	0.261 ± 0.009	52.715 ± 0.077
Urine 5	—	50	47.692 ± 0.073	95.38	—	47.570 ± 0.008

(–): not found.

3.2.3. Real Sample Analysis. This DPV method is used to analyze five actual human urine samples. To determine the method's accuracy, we spike each sample with 50 μM of DCF, and the relative recovery (Rev.) is calculated. All the values fall in the expectable range of 95.4–105% (Table 4). The content of DCF in the samples is also determined with the HPLC method for comparison. When $\alpha = 0.05$, the paired samples t-test proves that there is no statistically significant difference between the two methods ($p_{\text{two-tailed}} = 0.388\ (>0.05)$; $t(4) = 0.968$). These results demonstrate a good performance of the presented method for the determination of DCF in urine samples.

4. Conclusion

In this research, we successfully synthesized ZIF-67/g-C_3N_4 with the self-assembly method and used the material to modify a glassy carbon electrode for the electrocatalytic determination of diclofenac. The g-C_3N_4 is highly dispersed in ZIF-67 through an ultrasonic assisted stir to form a composite of g-C_3N_4 and ZIF-67. The enhancement of electrochemical signals is due to the synergic effect of ZIF-67 and g-C_3N_4. The oxidation of diclofenac on the modified electrode takes place with a two-electron-proton mechanism. The electrode process is controlled by adsorption. The proposed DPV method exhibits high sensitivity with a low detection limit and can be used to determine diclofenac at trace levels.

Data Availability

The data used to support the findings of this study are available from the corresponding author upon request.

Conflicts of Interest

The authors declare that they have no conflicts of interest.

Acknowledgments

This work was supported by the Hue University under the Core Research Program No. NCM.DHH.2019.08.

References

[1] J. A. Arancibia and G. M. Escandar, "Complexation study of diclofenac with β-cyclodextrin and spectrofluorimetric determination," *Analyst*, vol. 124, no. 12, pp. 1833–1838, 1999.

[2] M. Cleuvers, "Mixture toxicity of the anti-inflammatory drugs diclofenac, ibuprofen, naproxen, and acetylsalicylic acid," *Ecotoxicology and Environmental Safety*, vol. 59, no. 3, pp. 309–315, 2004.

[3] W. Jin and J. Zhang, "Determination of diclofenac sodium by capillary zone electrophoresis with electrochemical detection," *Journal of Chromatography. A*, vol. 868, no. 1, pp. 101–107, 2000.

[4] B. T. Alquadeib, "Development and validation of a new HPLC analytical method for the determination of diclofenac in tablets," *Saudi pharmaceutical journal*, vol. 27, no. 1, pp. 66–70, 2019.

[5] C. Arcelloni, R. Lanzi, S. Pedercini et al., "High-performance liquid chromatographic determination of diclofenac in human plasma after solid-phase extraction," *Journal of Chromatography. B, Biomedical Sciences and Applications*, vol. 763, no. 1–2, pp. 195–200, 2001.

[6] J. A. Arancibia, M. A. Boldrini, and G. M. Escandar, "Spectrofluorimetric determination of diclofenac in the presence of α-cyclodextrin," *Talanta*, vol. 52, no. 2, pp. 261–268, 2000.

[7] A. A. Ensafi, M. Izadi, and H. Karimi-Maleh, "Sensitive voltammetric determination of diclofenac using room-temperature ionic liquid-modified carbon nanotubes paste electrode," *Ionics*, vol. 19, no. 1, pp. 137–144, 2013.

[8] A. Sasal, K. Tyszczuk-Rotko, M. Wójciak, and I. Sowa, "First electrochemical sensor (screen-printed carbon electrode modified with carboxyl functionalized multiwalled carbon nanotubes) for ultratrace determination of diclofenac," *Materials*, vol. 13, no. 3, p. 781, 2020.

[9] A. Afkhami, A. Bahiraei, and T. Madrakian, "Gold nanoparticle/multi-walled carbon nanotube modified glassy carbon electrode as a sensitive voltammetric sensor for the determination of diclofenac sodium," *Materials Science and Engineering: C*, vol. 59, pp. 168–176, 2016.

[10] J. Qian, F. Sun, and L. Qin, "Hydrothermal synthesis of zeolitic imidazolate framework-67 (ZIF-67) nanocrystals," *Materials Letters*, vol. 82, no. 2012, pp. 220–223, 2012.

[11] Q. Yang, S. S. Ren, Q. Zhao et al., "Selective separation of methyl orange from water using magnetic ZIF-67 composites," *Chemical Engineering Journal*, vol. 333, pp. 49–57, 2018.

[12] Y. Li, Z. Jin, and T. Zhao, "Performance of ZIF-67 - Derived fold polyhedrons for enhanced photocatalytic hydrogen evolution," *Chemical Engineering Journal*, vol. 382, p. 123051, 2020.

[13] X. Wu, W. Liu, H. Wu et al., "Nanoporous ZIF-67 embedded polymers of intrinsic microporosity membranes with enhanced gas separation performance," *Journal of Membrane Science*, vol. 548, pp. 309–318, 2018.

[14] E. Sohouli, M. S. Karimi, E. M. Khosrowshahi, M. Rahimi-Nasrabadi, and F. Ahmadi, "Fabrication of an electrochemical mesalazine sensor based on ZIF-67," *Measurement*, vol. 165, p. 108140, 2020.

[15] X. Wang, K. Maeda, A. Thomas et al., "A metal-free polymeric photocatalyst for hydrogen production from water under visible light," *Nature Materials*, vol. 8, no. 1, pp. 76–80, 2009.

[16] J. Li, B. Shen, Z. Hong, B. Lin, B. Gao, and Y. Chen, "A facile approach to synthesize novel oxygen-doped g-C 3 N 4 with superior visible-light photoreactivity," *Chemical Communications*, vol. 48, no. 98, pp. 12017–12019, 2012.

[17] Y. Zhang, A. Thomas, M. Antonietti, and X. Wang, "Activation of carbon nitride solids by protonation: morphology changes, enhanced ionic conductivity, and photoconduction experiments," *Journal of the American Chemical Society*, vol. 131, no. 1, pp. 50-51, 2009.

[18] Z. Chen, S. Zhang, Y. Liu et al., "Synthesis and fabrication of g-C_3N_4-based materials and their application in elimination of pollutants," *Science of The Total Environment*, vol. 731, article 139054, 2020.

[19] S. C. Yan, Z. S. Li, and Z. G. Zou, "Photodegradation performance of g-C3N4 fabricated by directly heating melamine," *Langmuir*, vol. 25, no. 17, pp. 10397–10401, 2009.

[20] A. Thomas, A. Fischer, F. Goettmann et al., "Graphitic carbon nitride materials: variation of structure and morphology and their use as metal-free catalysts," *Journal of Materials Chemistry*, vol. 18, no. 41, pp. 4893–4908, 2008.

[21] M. J. Bojdys, J. Müller, M. Antonietti, and A. Thomas, "Ionothermal synthesis of crystalline, condensed, graphitic carbon nitride," *Chemistry - A European Journal*, vol. 14, no. 27, pp. 8177–8182, 2008.

[22] X. Bai, L. Wang, Y. Wang, W. Yao, and Y. Zhu, "Enhanced oxidation ability of g-C3N4 photocatalyst via C60 modification," *Applied Catalysis B: Environmental*, vol. 152, pp. 262–270, 2014.

[23] S. Tonda, S. Kumar, S. Kandula, and V. Shanker, "Fe-doped and -mediated graphitic carbon nitride nanosheets for enhanced photocatalytic performance under natural sunlight," *Journal of Materials Chemistry A*, vol. 2, no. 19, pp. 6772–6780, 2014.

[24] B. Long, J. Lin, and X. Wang, "Thermally-induced desulfurization and conversion of guanidine thiocyanate into graphitic carbon nitride catalysts for hydrogen photosynthesis," *Journal of Materials Chemistry A*, vol. 2, no. 9, pp. 2942–2951, 2014.

[25] K.-Y. A. Lin and W.-D. Lee, "Self-assembled magnetic graphene supported ZIF-67 as a recoverable and efficient adsorbent for benzotriazole," *Chemical Engineering Journal*, vol. 284, pp. 1017–1027, 2016.

[26] A. Awadallah-F, F. Hillman, S. A. Al-Muhtaseb, and H.-K. Jeong, "On the nanogate-opening pressures of copper-doped zeolitic imidazolate framework ZIF-8 for the adsorption of propane, propylene, isobutane, and n-butane," *Journal of Materials Science*, vol. 54, no. 7, pp. 5513–5527, 2019.

[27] Y. Jiao, D. Han, Y. Lu et al., "Characterization of pine-sawdust pyrolytic char activated by phosphoric acid through microwave irradiation and adsorption property toward CDNB in batch mode," *Desalination and Water Treatment*, vol. 77, pp. 247–255, 2017.

[28] C. M. Adeyeye and P.-K. Li, "Diclofenac sodium," in *Analytical profiles of drug substances*, vol. 19, pp. 123–144, Elsevier, 1990.

[29] A. J. Bard and L. R. Faulkner, "Fundamentals and applications," *Electrochemical methods*, vol. 2, no. 482, pp. 580–632, 2001.

[30] J. Soleymani, M. Hasanzadeh, N. Shadjou et al., "A new kinetic-mechanistic approach to elucidate electrooxidation of doxorubicin hydrochloride in unprocessed human fluids using magnetic graphene based nanocomposite modified glassy carbon electrode," *Materials Science and Engineering: C*, vol. 61, pp. 638–650, 2016.

[31] E. Laviron, "General expression of the linear potential sweep voltammogram in the case of diffusionless electrochemical systems," *Journal of Electroanalytical Chemistry and Interfacial Electrochemistry*, vol. 101, no. 1, pp. 19–28, 1979.

[32] C. Li, "Electrochemical determination of dipyridamole at a carbon paste electrode using cetyltrimethyl ammonium bromide as enhancing element," *Colloids Surfaces B Biointerfaces*, vol. 55, no. 1, pp. 77–83, 2007.

[33] K. G. Madsen, C. Skonberg, U. Jurva et al., "Bioactivation of diclofenac in vitro and in vivo: correlation to electrochemical studies," *Chemical Research in Toxicology*, vol. 21, no. 5, pp. 1107–1119, 2008.

[34] R. N. Goyal, S. Chatterjee, and B. Agrawal, "Electrochemical investigations of diclofenac at edge plane pyrolytic graphite electrode and its determination in human urine," *Sensors and Actuators B: Chemical*, vol. 145, no. 2, pp. 743–748, 2010.

[35] X. D. du, C. C. Wang, J. G. Liu et al., "Extensive and selective adsorption of ZIF-67 towards organic dyes: performance and mechanism," *Journal of Colloid and Interface Science*, vol. 506, pp. 437–441, 2017.

[36] F. Manea, M. Ihos, A. Remes, G. Burtica, and J. Schoonman, "Electrochemical determination of diclofenac sodium in aqueous solution on cu-doped zeolite-expanded graphite-epoxy electrode," *Electroanalysis*, vol. 22, no. 17-18, pp. 2058–2063, 2010.

[37] S. L. Z. Jiokeng, I. K. Tonle, and A. Walcarius, "Amino-attapulgite/mesoporous silica composite films generated by electro- assisted self-assembly for the voltammetric determination of diclofenac," *Sensors and Actuators B: Chemical*, vol. 287, pp. 296–305, 2019.

[38] F. Nasiri, G. H. Rounaghi, N. Ashraf, and B. Deiminiat, "A new electrochemical sensing platform for quantitative determination of diclofenac based on gold nanoparticles decorated multiwalled carbon nanotubes/graphene oxide nanocomposite film," *International Journal of Environmental Analytical Chemistry*, vol. 101, no. 2, pp. 153–166, 2021.

[39] M. M. Eteya, G. H. Rounaghi, and B. Deiminiat, "Fabrication of a new electrochemical sensor based on AuPt bimetallic nanoparticles decorated multi-walled carbon nanotubes for determination of diclofenac," *Microchemical Journal*, vol. 144, pp. 254–260, 2019.